JOURNAL OF GEOPHYSICAL RESEARCH, VOL. 112, E04006, doi:10.1029/2006JE002731, 2007

A magmatic loading model for coronae on Venus

Andrew J. Dombard,[1] Catherine L. Johnson,[2,3] Mark A. Richards,[4] and Sean C. Solomon[5]

Received 17 April 2006; revised 2 November 2006; accepted 29 November 2006; published 25 April 2007.

[1] Models for the formation of coronae, quasi-circular, volcanotectonic features on Venus, must explain four critical characteristics: coronae display (1) a wide range of diameters, (2) complex, varied topography, (3) fracture annuli, and (4) sometimes extensive volcanism. Previous models have difficulty simultaneously satisfying all four constraints. On the basis of observations and interpretations of features on Venus and Earth and experiments in geophysical fluid dynamics, we propose that coronae form in response to magmatic loading of the crust over zones of partial melting at the tops of thermally buoyant heads of transient mantle plumes that impinge on the base of the thermal lithosphere. By tying corona formation to a melt zone and not directly to an impinging upwelling, our conceptual model can account for the wide range in corona diameters. Lateral crustal flow, facilitated by magmatic heating, may lead to central depressions characteristic of many coronae. A thermomechanical, finite element simulation with a dissipating thermal anomaly leads to crustal thinning and predicts an elevation profile consistent with one of the more populous topographic classes of coronae. Deformation concentrated at the transition from thicker to thinner lithosphere above the thermal anomaly yields a narrow annulus of enhanced differential stress, consistent with formation of fracture annuli. Estimates of excess heat in an upwelling exceed the thermal energy in the melt that comprises the corona. Band-pass-filtered maps of the topography and gravity fields in the Beta-Atla-Themis region are consistent with upwellings now impinging on the lithosphere beneath seven coronae previously inferred to be active.

Citation: Dombard, A. J., C. L. Johnson, M. A. Richards, and S. C. Solomon (2007), A magmatic loading model for coronae on Venus, *J. Geophys. Res.*, *112*, E04006, doi:10.1029/2006JE002731.

1. Introduction

[2] Coronae, a class of quasi-circular, volcanotectonic features on Venus [*Stofan et al.*, 1997], were initially characterized by their distinctive tectonic signature consisting primarily of concentric fractures and ridges (Figure 1). An updated catalogue [*Stofan et al.*, 2001; *Glaze et al.*, 2002] lists 406 such features (known as Type 1). A further 107 coronae (known as Type 2) displaying more limited faulting have been identified primarily on the basis of topography. The topographic signatures of coronae are diverse and complex [*Smrekar and Stofan*, 1997]. Corona size is defined by the diameter of the fracture annulus (Type 1) or local topography (Type 2). The mean diameter is ~200–300 km; however, corona diameters can be as small as ~60 km and sometimes exceed 1000 km [*Glaze et al.*, 2002]. Volcanism associated with individual coronae is common but varied; largely constructional, volcanic features (e.g., small cones, domes, shields, and calderas) occur frequently inside the fracture annuli, while extensive flow deposits (nonconstructional) interior and exterior to the coronae are also observed for >40% of the corona population and cover areas up to 10^4–10^6 km^2 each [*Roberts and Head*, 1993; *Stofan et al.*, 1997, 2005]. Type 1 coronae are concentrated in a region defined by the Beta, Atla, and Themis volcanic rises (the BAT region), while Type 2 coronae have a more scattered distribution [*Stofan et al.*, 2001; *Glaze et al.*, 2002; *Johnson and Richards*, 2003]. Poor resolution of the gravity field generally prohibits identification of signatures associated with most individual coronae [*Johnson and Richards*, 2003]. Between 25% [*Johnson and Richards*, 2003] and just over 50% [*Hoogenboom et al.*, 2004] of coronae for which a gravity signal is resolved are interpreted to be locally compensated isostatically and are thus deduced to be inactive. Coronae inferred to be compensated have a scattered distribution, while those inferred to be uncompensated (and hence candidates for currently active features) are concentrated in the BAT region [*Johnson and Richards*, 2003]. Coronae tend to be absent near both positive and negative extremes of the

[1] Planetary Exploration Group, Space Department, Johns Hopkins University Applied Physics Laboratory, Laurel, Maryland, USA.
[2] Institute of Geophysics and Planetary Physics, Scripps Institution of Oceanography, La Jolla, California, USA.
[3] Also at Department of Earth and Ocean Sciences, University of British Columbia, Vancouver, British Columbia, Canada.
[4] Department of Earth and Planetary Science, University of California, Berkeley, California, USA.
[5] Department of Terrestrial Magnetism, Carnegie Institution of Washington, Washington, D.C., USA.

0148-0227/07/2006JE002731$09.00

Figure 1. Magellan radar image of Fatua Corona draped over Magellan gridded topography. The corona is viewed from the southeast. Boundaries of the image are 12°–21°S and 14°–22°E. Fatua Corona is ~400 km in diameter, although the main topographic high (~1.3 km at maximum) is ~300 km across. The high is surrounded by a moat and outer rim, and the characteristic fracture annulus is evident.

global geoid [*Johnson and Richards*, 2003]. Coronae are primarily found in three geologic settings: along chasmata and fracture belts, near volcanic rises, and as isolated features in the volcanic plains [*Stofan et al.*, 2001; *Glaze et al.*, 2002].

[3] Although corona formation models involving downwelling of lithospheric mantle have been proposed [e.g., *Hoogenboom and Houseman*, 2006], coronae usually have been interpreted as the products of upwardly buoyant mantle plumes on the basis of their characteristic faulting patterns and topographic signatures. Specific models range from plume impingement followed by gravitational relaxation [*Janes et al.*, 1992], to impingement or magmatic loading of an elastic lithosphere [e.g., *Cyr and Melosh*, 1993], to plume impingement with partial invasion into a low-density crust [*Koch and Manga*, 1996], to impingement-induced delamination of the lithosphere [*Smrekar and Stofan*, 1997]. Notably, the diameter of the corona is approximately the same diameter as the impinged plume in these models, implying a mantle convective regime that can create plume heads that range in size from several tens to perhaps a thousand kilometers across. There is disagreement on whether the origin of the plume buoyancy is thermal, compositional, or both. Some models invoke purely thermal buoyancy [e.g., *Smrekar and Stofan*, 1997], others invoke melt (compositional) diapirs [e.g., *Tackley and Stevenson*, 1991, 1993], and still others include both sources [e.g., *Hansen*, 2003]. Each of these models captures some aspect of the characteristics observed in the corona population. For instance, the model of *Smrekar and Stofan* [1997] reproduces the wide range of topographic types.

[4] In this paper, we propose that coronae on Venus are products of magmatic loading of the crust above transient thermal plume heads in the mantle. We begin by examining four critical characteristics of the corona population and their implications for formational models. In section 3, we review the physics of bottom-heated convection that may apply to Venus and then describe our corona formation model. Tests of the model are provided in four subsections. In section 4, we discuss how the new model may simultaneously satisfy the four key observations of the corona population, and how other models do not. We conclude with some remarks on directions for future research.

2. Critical Observations and Implications for Models

[5] There are four critical observations of the corona population that have distinct implications for any model of their formation. First, coronae have a wide range of diameters (~60 km to > 1000 km) that are well fit by a lognormal distribution with a mean of ~200–300 km (Figure 2), suggesting, but not demonstrating, a single formational mechanism [*Glaze et al.*, 2002]. Second, coronae display complex and varied topographic signatures; nine distinct topographic types have been defined [*Smrekar and Stofan*, 1997], although the two most populous types (~45% of the total population) exhibit elevated rims surrounding central regions that are elevated and flat, domed, or depressed below the background elevation. Third, most coronae have distinctive annular concentrations of narrowly spaced extensional fractures; consequently, any model must be able to predict sufficient stresses of the proper orientation. Fourth, while many coronae have limited associated volcanism [e.g., *Martin et al.*, 2005], volcanism associated with coronae is often extensive and sometimes comparable in scale to terrestrial flood volcanism [*Roberts and Head*, 1993; *Stofan et al.*, 1997, 2005]. Moreover, for many volcanic environments on Earth, the volume of intrusive magmatism exceeds that of surface volcanism by a factor of three or more [e.g., *Crisp*, 1984]. It is thus reasonable to

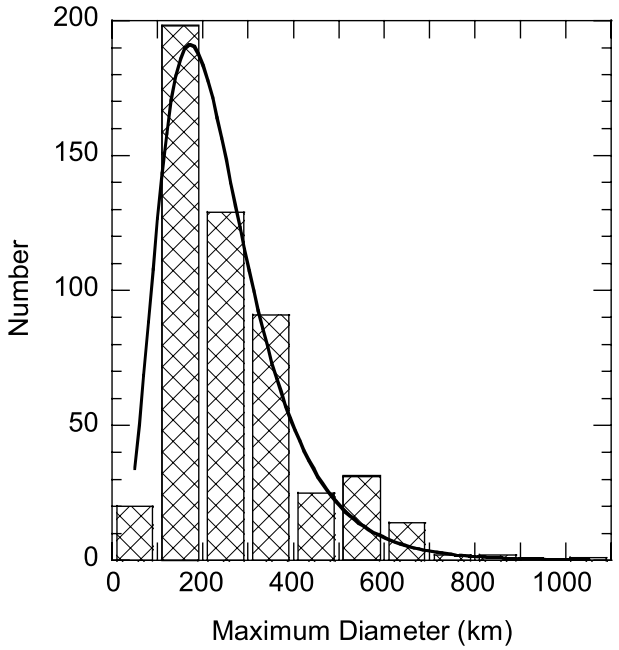

Figure 2. Histogram of maximum diameters for both Type 1 and Type 2 coronae (data from *Stofan et al.* [2001] and *Glaze et al.* [2002]), binned every 100 km. A fit of a lognormal distribution is also shown, with geometric and arithmetic means of ~217 km and ~243 km, respectively.

expect that both extrusive and intrusive magmatism (crustal injection and underplating) may be significant in any corona formation scenario and should be predicted by corona formation models.

3. Coronae as Products of Melt Intrusion

[6] We propose a conceptual framework for corona formation that may satisfy all four observations above [cf. *Dombard et al.*, 2002, 2006], although this possibility should be tested more thoroughly than the initial tests we provide here. We begin by reviewing the physics of bottom-heated convection that may apply to the mantle of Venus. A common thread of nearly all corona formation models is that they are the end result of a buoyant upwelling impinging on the lithosphere and crust of Venus; the source of this buoyancy is usually inferred to be excess temperature. The physics of a mantle system characterized by thermal upwelling is simple in principle, though in practice complex and the subject of intensive, ongoing research [e.g., *Leitch and Davies*, 2001; *Lithgow-Bertelloni et al.*, 2001; *Farnetani et al.*, 2002; *Jellinek et al.*, 2002, 2003; *Gonnermann et al.*, 2004; *Jellinek and Manga*, 2004; *Robin et al.*, 2004, 2006; *Davaille and Vatteville*, 2005]. Bottom heating of a viscous fluid produces a thermal boundary layer, and buoyant instabilities in this layer form upwellings that ascend through the fluid. If cooling of the bulk fluid is efficient, the boundary layer will be strong, with a viscosity contrast of perhaps several orders of magnitude. This state is often viewed to be representative of the dynamics of the Earth's mantle, where heat from the core forms a strong (high excess temperature) boundary layer because of relatively efficient cooling by plate tectonics. The resultant upwelling state is characterized by long-lived mantle plumes that can, though not always [e.g., *Davaille and Vatteville*, 2005], remain connected to the bottom boundary layer via a tail. Venus, on the other hand, lacks modern plate tectonics and resides in the "stagnant-lid" convective regime [*Solomatov and Moresi*, 1996]. Dynamically, a bottom-heated system with inefficient cooling produces a somewhat thinner, weaker boundary layer. The resultant instabilities produce upwellings that are smaller (though still large enough to ascend through the mantle before being halted by thermal diffusion), possess lower excess temperatures and viscosity contrasts, and are less likely to remain connected by a tail to the boundary layer as they rise. This type of upwelling has been referred to as a thermal [e.g., *Jellinek et al.*, 2002; *Jellinek and Manga*, 2004], to differentiate it from the long-lived mantle plume. Furthermore, laboratory experiments suggest that the transition from the strong boundary-layer state to a weak state is characterized by both kinds of structures [*Robin et al.*, 2004, 2006], where somewhat larger-scale flow due to plumes may focus the ascent of the thermals [*Lithgow-Bertelloni et al.*, 2001; *Jellinek et al.*, 2003; *Gonnermann et al.*, 2004].

[7] While this transitory state is poorly understood, its existence may help explain the distribution of coronae on Venus. *Johnson and Richards* [2003] proposed that plume behavior in the mantle of Venus is characterized by a few large, long-lived plumes, which generate volcanic rises, and more numerous, smaller thermals, which form coronae. Flow associated with plumes focuses the ascent of thermals, accounting for the concentration of uncompensated coronae in the BAT region. Thermals in the immediate vicinity of large, established plumes tend to be captured entirely. Thus, isolated thermals are generally excluded from the long-lived structures, both upwelling or downwelling, possibly explaining why coronae tend to be absent near positive (rises such as Atla and Beta) and negative (lowland plains) extremes in the gravity field of Venus, interpreted as marking major upwellings and downwellings in the mantle [*Simons et al.*, 1997; *Lawrence and Phillips*, 2003]. Incomplete assimilation of thermals into plumes may explain the presence of corona-dominated rises [*Stofan et al.*, 1995; *Smrekar and Stofan*, 1999].

[8] Volcanic rises on Venus are approximately 2000 km across [*Smrekar et al.*, 1997], which suggests that the plume heads were $\sim$1000 km across prior to impingement on the lithosphere. This size is comparable to large, long-lived terrestrial plumes such as Hawaii and Iceland [e.g., *Leitch and Davies*, 2001; *Farnetani et al.*, 2002]. Terrestrial plumes are thought to have excess temperatures of several hundred Kelvin; given the correspondence in sizes of terrestrial and Venus plumes, we assume a similar excess temperature for plumes on Venus. Thermals arise from regions of the boundary layer that are (locally) thinner and weaker than that for the plumes. The thermals cannot be much less in diameter than the plumes because the rise time through the mantle and the thermal diffusion time of a thermally buoyant upwelling both scale with the square of the size, yielding a sharp cut-off in the diameter of upwellings that can ascend through the mantle; indeed, this observation argues against models that tie the diameter of a thermally buoyant upwelling ascending through the entire mantle directly to the size of the resultant corona [e.g., *Hansen*, 2003]. We therefore assume a typical diameter of $\sim$500–1000 km and an excess temperature of $\sim$100–300 K for the thermals within the mantle of Venus.

[9] Alternative models have been proposed for the state of the mantle of Venus (e.g., the layered-mantle model of *Stofan and Smrekar* [2005]), but regardless of the precise state (although we focus the following discussion on thermals), we propose that it is the interaction with the crust of the melt generated at the top of the upwelling, and not the impingement of the upwelling on the base of the lithosphere, that produces the main observable features associated with coronae. As shown schematically in Figure 3, a thermal initially less than 1000 km in diameter [e.g., *Farnetani et al.*, 2002; *Jellinek et al.*, 2002] impinges on the base of a thermal lithosphere of order 100 km thick [e.g., *Phillips and Hansen*, 1998]. Upon impingement, the thermal flattens and is widened by a factor of $\sim$2–2.5 [e.g., *Koch and Manga*, 1996; *Leitch and Davies*, 2001; *Farnetani et al.*, 2002], forming broad-scale dynamic topography of order 0.1–1 km (not shown in Figure 3). Partial melt forms at the top center of the thermal [e.g., *Leitch and Davies*, 2001; *Farnetani et al.*, 2002], where the combination of highest excess temperatures and lowest pressures results in conditions most favorable to decompression melting. Unlike the thermal itself, the size of the pocket of partial melt is highly sensitive to local variables such as excess temperature and lithospheric thickness. Consequently, small coronae may

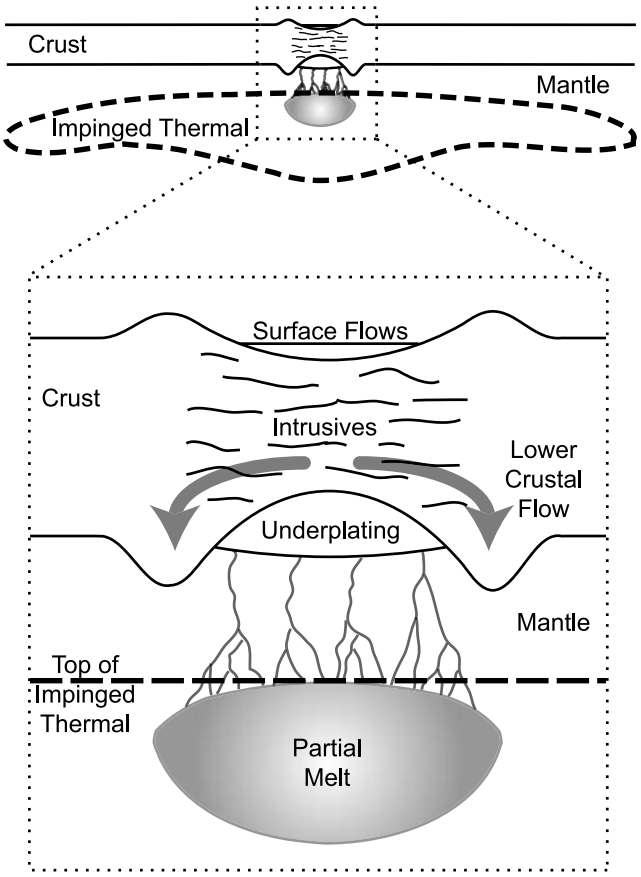

Figure 3. Schematic cross section of the corona formation model. Scales, particularly horizontal versus vertical and the vertical distance between the top of the thermal (~100 km deep) and the base of the crust (~30 km deep), are exaggerated.

form over limited pockets of melt, while larger coronae form from volumetrically larger pockets of melt that span a greater fraction of the width of the impinging thermal. The present-day thermal lithosphere is likely thicker than the crust [*Grimm and Hess*, 1997; *Phillips and Hansen*, 1998], so this melt must rise through the lithospheric mantle, for example, via corrosive etching [*Spiegelman et al.*, 2001; *Beck et al.*, 2006] in the warm lower lithospheric mantle or through dikes in the cooler, upper parts, to the point where it loads the crust by underplating [e.g., *Caress et al.*, 1995], intrusion, or extrusion. A corona that is observed on the surface is then the product of this magmatism and the response of the lithosphere to these magmatic loads. This geometrically simple picture can be complicated by compositional variations and stresses within the lithospheric mantle and crust [e.g., *Sleep et al.*, 2002], which might explain the approximately quarter of the corona population that are markedly noncircular or found in multiples [*Stofan et al.*, 1992].

3.1. Melting and the Energy Budget

[10] A central issue is whether the thermals can generate enough melt to produce coronae. We can address this issue via energy budget considerations [cf. *Watson and McKenzie*, 1991]. The excess thermal energy can be estimated as the product of the thermal's volume, density, specific heat, and excess temperature. For a spherical thermal 500 km across, a mantle density of 3300 kg m^{-3}, a specific heat of 1000 J kg^{-1} K^{-1}, and an excess temperature of 100–300 K, the energy available is 10^{25}–10^{26} J. Similarly, the thermal energy in the magma needed to make a corona can be estimated as the product of the volume of melt, the melt density (~2700 kg m^{-3}), and the latent heat of fusion, taken to equal that of basalt (~4×10^5 J kg^{-1}). Under our scenario, the surface topography of a corona arises from the addition of magma, both on and intruded beneath the surface. To approximate the total volume of this magma, we combine this intrusion and extrusion into an equivalent cylindrical disk with a diameter equal to the corona's diameter D and a height h. Though the topographic signature is complex, the topographic relief is typically ~1 km. To account for partial compensation via Airy isostasy or dense intrusive material, we consider a range of h between 1 and 10 km. We show the resultant thermal energy as a function of corona diameter in Figure 4, which demonstrates that the energy in the melt that leads to a corona is generally a very small fraction of the excess energy available in a thermal in the mantle of Venus and only approaches comparability for large-diameter coronae and very thick magmatic stacks. Thus our proposed

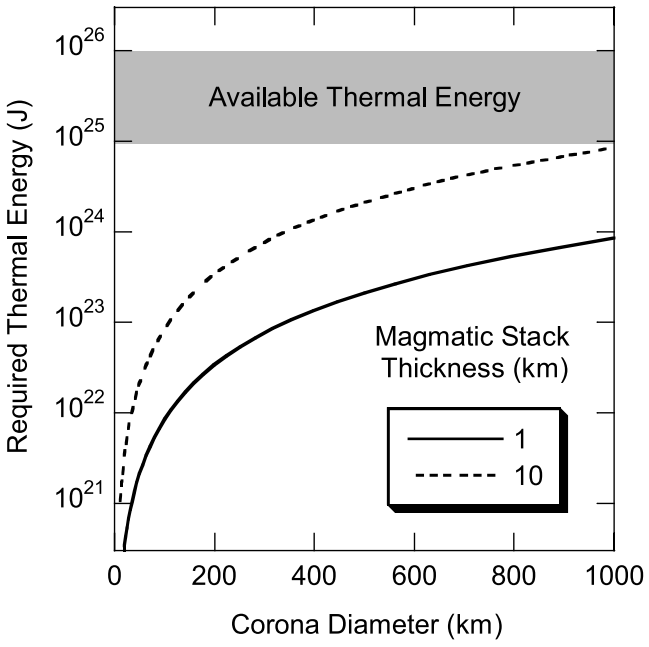

Figure 4. Thermal energy in the melt required to make a corona, as a function of corona diameter. The volume of magma leading to corona formation is estimated as that of a disk with the same diameter as the corona and a thickness of 1 (solid line) to 10 (dashed line) km. The shaded zone represents the excess thermal energy in the mantle upwelling that produces the partial melt. The generally large difference demonstrates that sufficient energy is available to produce the melt invoked in our proposed corona formation scenario.

scenario is consistent with the energy available in the system.

3.2. Topography and Lower Crustal Flow

[11] By our hypothesis, the topographic signature of a corona is plausibly the result of this magmatism and subsequent deformation of the mechanical lithosphere. An associated issue is how to explain coronae with central zones lower than the elevation of background terrain after volcanic material has been added to the crust. Such an outcome is reported in the terrestrial literature; *Diakov et al.* [2002] noted subsidence over magmatic intrusions in the Siberian Traps, although these depressions are of a smaller scale (~100 km across) and inferred to form from collapse of magma chambers. Because high surface temperatures and a thick crust on Venus [*Grimm and Hess*, 1997] result in elevated temperatures in the lower crust, we suggest that crustal thinning due to lateral flow may be a possible solution; crustal thinning has also been noted at the Siberian Traps [*Pritula et al.*, 1974]. The combination of crustal underplating and positive surface topography (volcanic flows or crust uplifted by magmatic intrusions) will pinch the original crust, inducing lateral flow and thinning. A crustal underplate, possibly a cumulate that is denser than basalt [e.g., *Farnetani et al.*, 1996], and a thinned original crust could result in a crustal stack that is denser than prior to the corona, resulting in a net downward load and a central depression. An intense thermal pulse from the magmatism to the crust directly beneath the forming corona will facilitate this flow (enhancement to the regional heat flow associated with the impinged thermal is far less important because of the greater depth and smaller temperature contrast).

[12] We estimate relevant timescales using the lower crustal flow model of *Nimmo and Stevenson* [2001]. The characteristic timescale for horizontal thinning is given by the ratio of the width of the zone of flow (here, the corona diameter) to the horizontal flow velocity. This flow velocity is proportional to the horizontal pressure gradient, the thickness of the flow channel, and the inverse of the viscosity. Thus it is straightforward to show that the timescale is

$$\tau = \frac{D^2 \eta_{eff}}{\Delta \rho g \delta^3}, \tag{1}$$

where D is the corona diameter, η_{eff} is the effective viscosity, $\Delta\rho$ is the density contrast, and g is gravitational acceleration. The thickness of the flow channel δ is given by

$$\delta = \frac{Rk(T_s + F_o t_c/k)^2}{QF_0} \tag{2}$$

where R is the universal gas constant, k is the thermal conductivity, T_s is the surface temperature, F_o is the heat flow into the base of the crust, t_c is the crustal thickness, and Q is the activation energy of the ductile flow law [cf. *Nimmo and Stevenson*, 2001, equation (14)]. The surface temperature on Venus is currently 740 K, and the present-day global heat flow is estimated at ~40–50 mW m^{-2} [*Phillips and Hansen*, 1998]. For a thermal conductivity of the crust of 2.5 W m^{-1} K^{-1}, temperatures at the base of a crust ~30 km thick [*Grimm and Hess*, 1997] in equilibrium with the global heat flow are ~1220–1340 K. The melting point of natural peridotite at a pressure equivalent to ~100 km depth in Venus is ~1740 K [*Hirschmann*, 2000]; we assume that this is the temperature of the magmas intruding into the crust. Because of a trade-off between temperature at its base and the temperature contrast across the crust, the channel thickness is generally ~5% of the crustal thickness for both a crust subjected only to the global heat flow and one with underplating magmatism (i.e., melting) at its base. The channel could be thicker, however, because intrusive magmatism within the crust will deposit heat locally, a situation not captured by *Nimmo and Stevenson* [2001]. For D = 250 km, $\Delta\rho$ = 200 kg m^{-3} (intermediate between mantle and crustal rocks and thus appropriate to the density contrast between magma cumulates and the surrounding country rock), g = 8.87 m s^{-2}, a flow channel thickness of 1.5, 5, or 15 km, and an effective viscosity appropriate to anhydrous Maryland diabase [*Mackwell et al.*, 1998], we show timescales for lower crustal flow as functions of effective channel temperature in Figure 5. Timescales using the faster flow law for anhydrous Columbia diabase [*Mackwell et al.*, 1998] would be about an order of magnitude shorter. For comparison, the conductive cooling time of the crust is ~30 Myr, and corona formation times have been estimated to be millions to hundreds of millions of years [*Stofan et al.*, 2005]. The timescale for lateral flow is less than these timescales for the thicker channels and for plausible temperatures. Consequently, the thermal anomaly accompanying magmatic intrusion into the deep crust

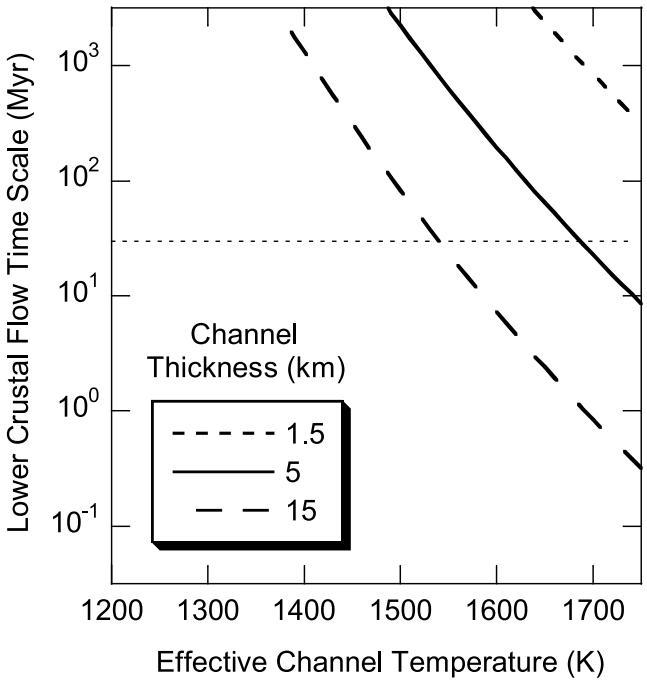

Figure 5. Timescales for lower crustal flow as functions of flow channel temperature for three channel thicknesses. For reference, the horizontal dashed line marks 30 Myr, the approximate conductive timescale of a crust ~30 km thick.

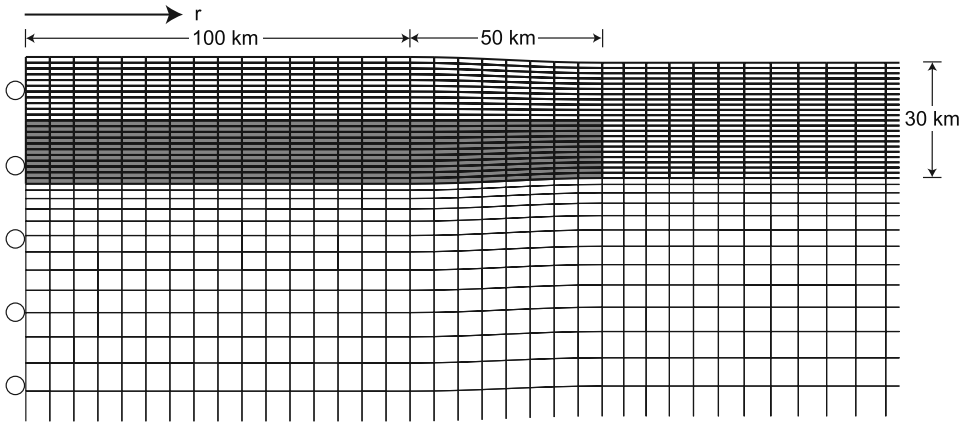

Figure 6. A portion of the mesh used the in the thermomechanical, finite element simulation of corona deformation. Elements with thicker grid lines are assigned parameters appropriate to the crust, whereas elements with thinner grid lines are assigned parameters appropriate to the mantle (see Table 1). Within a grey zone spanning the radius of the corona and extending from the crust-mantle interface to the top of the lower crust, initial temperatures are constrained to simulate the thermal anomaly associated with magmatic intrusion. A free-slip condition applied to the central axis of the axisymmetric system in the mechanical analysis is denoted by "rollers" on the left side.

could facilitate crustal thinning. Conversely, the lower crust on the periphery of the intrusion would remain cooler and stiffer and would likely impede the lateral flow, resulting in a thickened annulus of crust and hence the production of a topographic rim. Furthermore, this thinning process is consistent with the observation that more of the smaller coronae tend to possess central depressions than larger ones [*Glaze et al.*, 2002]. Channelized flow is more efficient for thicker channels (see equation (1)); for a given crustal thickness, a smaller corona has a thicker channel relative to its diameter.

3.3. A Thermomechanical, Finite Element Test

[13] To test our proposed scenario and supporting estimates further, we perform a thermomechanical, finite element simulation of the response of the lithosphere of Venus to magmatic loads. We use the MSC.Marc finite element package (http://www.mscsoftware.com), which we have applied to other geophysical problems, including thermomechanical simulations and an assessment of thinning of crustal plateaus on Venus [*Nunes et al.*, 2004; *Dombard and Phillips*, 2005; *Dombard and McKinnon*, 2006a, 2006b]. Our simulation is geometrically simple, modeling one radial-vertical plane for an axisymmetric corona ~250 km in diameter (Figure 6 and Table 1). The crust is initially 30 km thick [*Grimm and Hess*, 1997]. The load on the lithosphere arises from thickened crust, volcanically emplaced as surface flows, intracrustal injections, and an underplate. The surface topography is modeled as a flat-topped plateau 1.5 km tall; at the edge of the plateau, the elevated terrain transitions to the elevation of the background terrain at radial distances between 100 and 150 km via a cosine function. The maximum edge slope is ~2.7°, and the average slope is ~1.7°. Topography on the crust-mantle boundary is modeled as a similarly shaped, though vertically inverted, 1.5-km-thick layer on the base of the crust. We do not directly simulate the mechanical consequences of intrusive magmatism or the deformation associated with the initial volcanic displacement of mantle material. The far boundary is placed 700 km from the central axis, while the bottom boundary is 500 km deep. The entire simulated space is divided into ~4600 elements concentrated toward the crust where most of the deformation will occur.

[14] Our thermomechanical simulation is uncoupled; that is, the thermal solution is obtained first and then

Table 1. Parameters in the Finite Element Simulation

Parameter	Value
Geometry	
Corona radius	~125 km
Maximum surface topography	1.5 km
Maximum crust-mantle topography	1.5 km
Baseline crustal thickness	30 km
Maximum edge slope	~2.7°
Mesh width	700 km
Mesh depth	500 km
Thermal Analysis	
Surface temperature	740 K
Basal heat flow	45 mW m^{-2}
Thermal diffusivity	10^{-6} m^2 s^{-1}
Thermal conductivity, crust	2.5 W m^{-1} K^{-1}
Thermal conductivity, mantle	4 W m^{-1} K^{-1}
Thermal anomaly initial temperature	1640 K
Duration until anomaly constraint removed	1 Myr
Mechanical Analysis	
Gravitational acceleration	8.87 m s^{-2}
Density, crust	2900 kg m^{-3}
Density, mantle	3300 kg m^{-3}
Poisson's ratio	~0.5
Young's modulus, crust	56 GPa
Young's modulus, mantle	120 GPa
Crust ductile rheology	anhydrous diabase[a]
Mantle ductile rheology	anhydrous olivine[b]
Minimum viscosity limit	10^{20} Pa s

[a] *Mackwell et al.* [1998].
[b] *Karato and Wu* [1993].

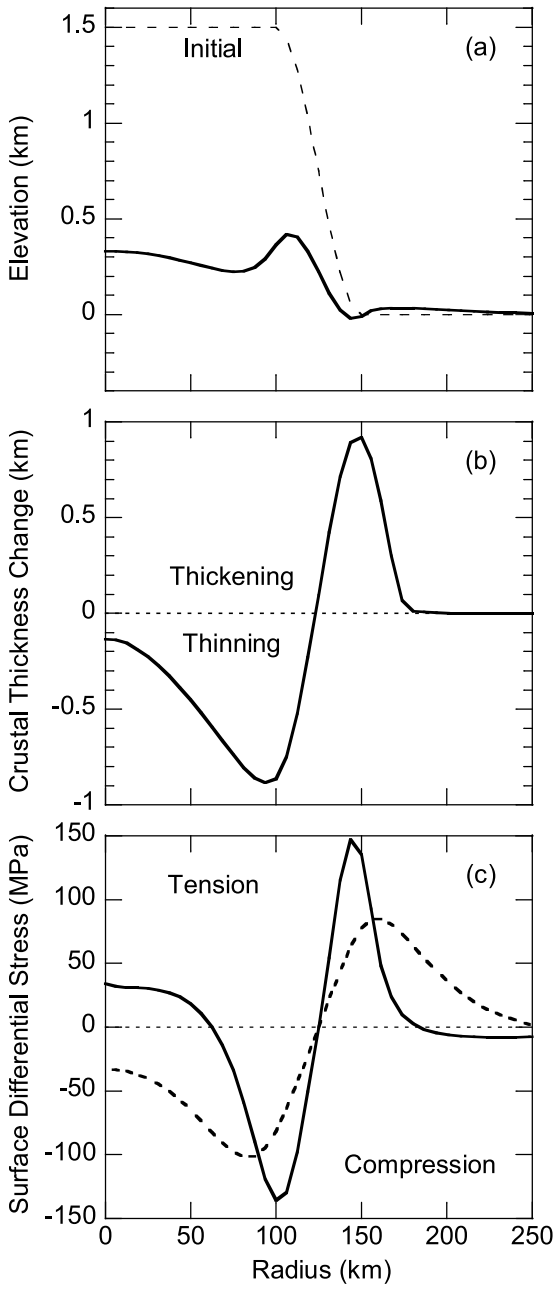

Figure 7. Results from a thermomechanical, finite element simulation (see text for description). (a) The surface topography is consistent with corona topographic Group 3 [*Smrekar and Stofan*, 1997]. (b) A crustal thickness profile demonstrates thinning facilitated by a thermal anomaly accompanying magmatic intrusion. Lower temperatures outward of the thermal anomaly lead to peripheral thickening. (c) A profile of surface differential stress displays a zone of large radial tensile stresses, which may account for the fracture annuli around coronae. Flexure and a transition from thinner to thicker lithosphere at the edge of the thermal anomaly yield a stress profile (solid line) that is larger in magnitude and more narrowly confined in radial distance than a case with no thermal anomaly (dashed line).

used in the mechanical solution. We do not track advection of heat with the deforming material, although we recognize that this process may become important for large degrees of lower crustal flow. Thermal parameters are listed in Table 1. We apply a surface temperature of 740 K and a basal heat flow of 45 mW m^{-2} [e.g., *Phillips and Hansen*, 1998]; heat flow through the sides of the finite element mesh is restricted. To simulate bulk heating due to intrusive magmatism that likely occurs as a series of discrete events at a smaller scale than the resolution of the finite element mesh, a subsurface thermal anomaly, 150 km in radius and extending upward from the underplated material to the top of the lower crust (i.e., 15 km depth), is implemented by constraining all the nodes within the boundary of the anomaly to an initial temperature of 1640 K (i.e., lower than the assumed temperature of the melt). From Figure 5 the timescale for lower crustal flow is $\sim$2 Myr. The simulation begins in equilibrium with the thermal anomaly, but after 1 Myr, a lower estimate for the formation time of a corona [*Stofan et al.*, 2005], the temperature constraint within the thermal anomaly is removed. The system then conductively cools toward equilibrium with the surface temperature and the heat flow.

[15] For the mechanical part, the simulation is run under a complete large-strain formulation; parameters for the mechanical analysis are also listed in Table 1. Loading is accomplished by means of an applied gravitational body force with an acceleration of 8.87 m s^{-2}. Free-slip boundary conditions are applied to the sides of the mesh, while the nodes on the bottom of the mesh are locked. The mantle has a density of 3300 kg m^{-3}, and the crustal density is 2900 kg m^{-3}. The surface load and the underplate are assigned the same mechanical parameters as the crust. The simulation employs a viscoelastic rheology; because we wish to assess stress magnitudes, we do not include plasticity, a continuum approximation for discrete, brittle faulting that would limit stresses to a yield strength [cf. *Dombard and Phillips*, 2005]. For the elastic parameters, we would nominally use a Poisson's ratio of 0.25 and Young's moduli of 70 GPa for the crust and 150 GPa for the mantle; to prevent gravitational self-compression, however, we set Poisson's ratio near its incompressibility limit of 0.5 and decrease the nominal values of the Young's moduli by a factor of 4/5, thereby preserving the flexural rigidity of the material [*Dombard and McKinnon*, 2006b]. We have verified with MSC.Marc that this technique reproduces deflections from an analytic solution of a simple elastic-flexure problem [e.g., *Turcotte and Schubert*, 1982, pp. 116–117] and in a lithospheric flexure case similar to the one presented in Figures 6 and 7 but for a compositional half-space (all crustal material), an invariant thermal state with no thermal anomaly, and a simpler loading scheme (a normal force applied to the surface equivalent to $\sim$1 km of material). Differences in the surface displacement are negligible. Subsurface stresses are likewise similar, although surface stresses are augmented by up to 20%. A formulation that enforces calculation of volumetric strain at element centroids prevents numerical errors that can arise in nearly incompressible, viscoelastic finite element simulations. For the viscosity, we use parameters for dislocation creep of anhydrous Maryland

diabase [*Mackwell et al.*, 1998] for the crust and of anhydrous olivine [*Karato and Wu*, 1993] for the mantle. To keep the computation time of the simulation tractable (several days), we limit the minimum viscosity to a value of 10^{20} Pa s. For the case illustrated in Figure 5, the flow channel viscosity is $\sim 10^{19}$ Pa s; lower crustal flow in the simulation is therefore inhibited.

[16] Results from this simulation are shown in Figure 7. Taken together, they encompass many aspects observed in the corona population. The results are shown after a simulated time of 10 Myr; results after 100 Myr are similar because most of the deformation occurs while the thermal anomaly is present. The topography (Figure 7a) is similar to that of the Group 3 coronae of *Smrekar and Stofan* [1997], a rim surrounding an interior high or domed interior, the second-most-populous topographic group that includes ~21% of the corona population. This simulation also predicts a flexurally induced moat. While moats are observed around some coronae [e.g., *Johnson and Sandwell*, 1994; *Smrekar and Stofan*, 1997], the lack of a moat could conceivably be due to burial by volcanic flooding.

[17] The simulation predicts some crustal thinning (Figure 7b). The greatest thinning occurs near the inside edges of the loads; because of higher viscosities in the lower crust outward of the thermal anomaly, this crustal material collects along the outside edges of the loads, resulting in peripheral thickening. This thickening augments the formation of the topographic rim. The higher lateral viscosity bottleneck limits the amount of crustal thinning that might be expected from the model of *Nimmo and Stevenson* [2001], which assumes a flow channel of infinite lateral extent. Other aspects of the simulation (selection of the stronger flow law of Maryland diabase over that of Columbia diabase [*Mackwell et al.*, 1998], the applied minimum viscosity, and removal of the thermal anomaly constraint before the characteristic flow time) also limit thinning.

[18] Surface radial stress is shown in Figure 7c. Peak radial tensile stresses near the topographic rim exceed 145 MPa (120 MPa after adjustment for the ~20% augmentation because of the assumption of nearly incompressible elastic behavior), well above inferred fault strengths on Venus of 10 to perhaps 80 MPa [*Barnett and Nimmo*, 2002]; thus a corona-like annulus of extensional fractures is predicted. The transition from thinner lithosphere over the thermal anomaly to thicker lithosphere along the periphery concentrates the flexural deformation, resulting in a stress profile that is narrow in radial extent and consistent with the narrow widths of the fracture annuli. Conversely, a stress profile from a simulation without a thermal anomaly is broader, in addition to being weaker and perhaps just barely above fault strengths on Venus. Thus, the presence of the thermal anomaly may be critical to the formation of the fracture annulus. A similar effect was observed in simulations of deformation beneath the Tharsis Montes on Mars [*Dombard and Phillips*, 2005].

3.4. Evidence in the Topography and Gravity

[19] If coronae form in response to thermals impinging on the base of the lithosphere, then a signal from the dynamic topography and the low-density anomaly of the impinged upwelling might be expected in the topography and gravity fields at those coronae that are actively forming. This signal should be of a longer length scale than the corona itself. The difficulty with observing such signals is that they are superposed on other higher-amplitude features of longer, comparable, and shorter length scales. To identify signatures of impinged thermals, we can filter the topography and gravity fields to possess only appropriate length scales. As discussed above, an initially spherical thermal will widen by a factor of ~2–2.5 upon impingement on the thermal lithosphere. A thermal initially 500–1000 km across will, after impingement, be ~1000–2500 across, corresponding approximately to spherical harmonic degrees 15–40.

[20] Similarly, we can predict the magnitude of the topographic, geoid, and gravity anomaly signals. We estimate the scale of the dynamic topography by equating the buoyancies of the impinged thermal and the uplifted surface. The density anomaly of the thermal will be ~10–30 kg m^{-3} for a mantle density of 3300 kg m^{-3}, a volumetric thermal expansion coefficient of 3×10^{-5} K^{-1}, and an excess temperature of ~100–300 K. By conservation of volume, an impinged thermal initially 500–1000 km across will be of order 100 km thick. Balancing the resultant buoyancy with an uplifted surface yields a magnitude of the dynamic topography of 0.1–1 km. This topography on both the surface and the crust-mantle boundary, in addition to the low density of the thermal, will produce a geoid anomaly. Following *Banerdt* [1986], for a representative spherical harmonic degree of 30 the geoid anomaly will be positive and have a magnitude of order 10 m. In addition, a Bouguer gravity anomaly will be produced by the positive density anomaly associated with the uplifted crust-mantle boundary and the negative density anomaly of the thermal. From an upward-continued Bouguer gravity formula [e.g., *Turcotte and Schubert*, 1982], the gravity signal from the thermal tends to dominate over the signal from the crust-mantle boundary, producing a 10–100 mgal negative anomaly.

[21] Band-pass-filtered maps of the topography, geoid, and Bouguer gravity anomaly in the BAT region are shown in Figure 8. The fields have been filtered between spherical harmonic degrees 15 and 44 with a cosine taper applied to degrees 41–44 to reduce ringing. The spherical harmonic coefficients of the topography and gravity are taken from the NASA Planetary Data System (http://pds-geosciences.wustl.edu/missions/magellan/shadr_topo_grav/index.htm), and we adopt the finite-amplitude method of *Wieczorek and Phillips* [1998] to determine the topographic correction used in the construction of the Bouguer anomaly map. The scales of the maps are selected to be consistent with the predicted magnitudes of the anomalies arising from the impingement of thermals. Superimposed on the maps are the locations of all Type 1 and Type 2 coronae from the database of *Stofan et al.* [2001] and *Glaze et al.* [2002]. There are seven coronae (all Type 1 and marked in Figure 8 with larger symbols) that simultaneously coincide with positive topographic and geoid anomalies and negative Bouguer anomalies. It is noteworthy that these coronae are all smaller than the scales to which the maps have been filtered; the signals instead come from larger-scale features beneath the coronae. We infer then that these coronae (Table 2) are presently underlain by impinged thermals and are geologically active.

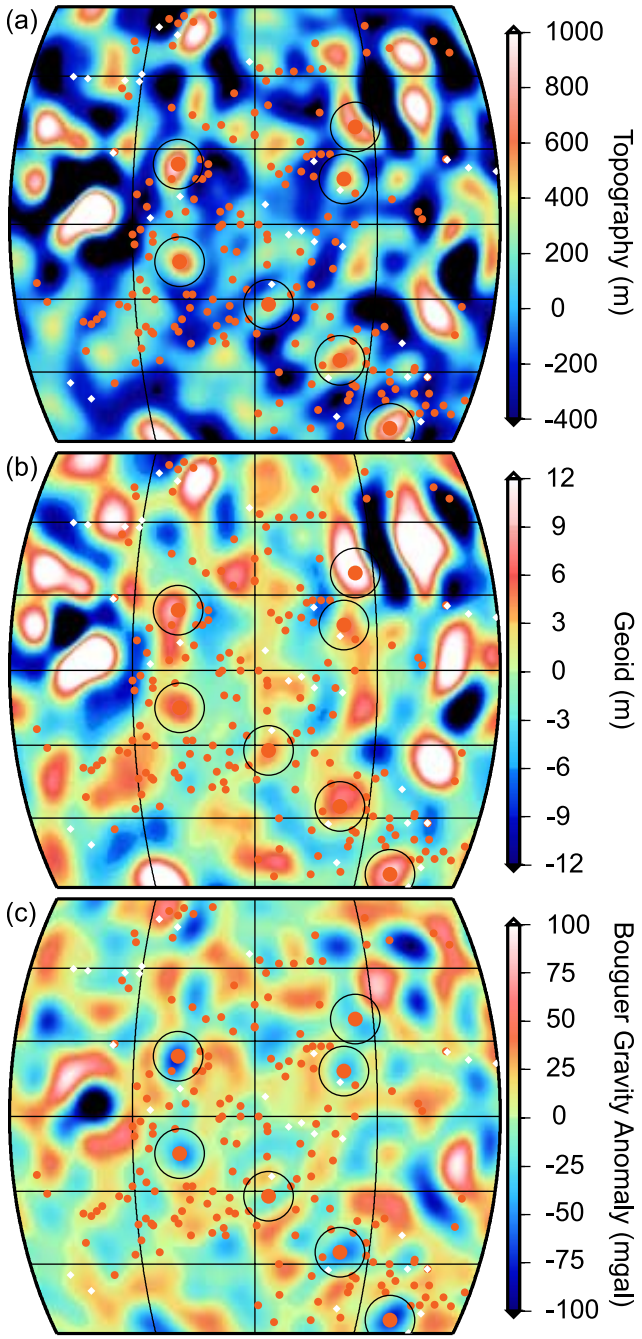

Figure 8. Maps of the (a) topography, (b) geoid, and (c) Bouguer gravity anomaly, in the Beta-Atla-Themis region of Venus band-pass-filtered between spherical harmonic degrees 15 and 44 with a cosine taper applied to degrees 41–44 to reduce ringing. The maps are in the Mollweide projection and span latitudes 45°N to 45°S and longitudes 180° to 300°E. Red circles and white diamonds mark the positions of Type 1 and Type 2 coronae. Larger red circles denote those coronae that simultaneously sit on positive topographic and geoid anomalies and negative Bouguer anomalies; these coronae are inferred to be underlain by presently impinged thermals and thus may be geologically active. The black circles around the active coronae indicate a reference scale of ~1000 km diameter.

[22] There is additional evidence that these coronae are active. All seven were also identified by *Johnson and Richards* [2003] as candidates for currently active features on the basis of their inferred uncompensated state. Furthermore, if these coronae are active their volcanic flows should be some of the youngest units in local geologic maps. Two of these coronae, Atete and Maram, are located within the boundaries of published geologic maps of the Galindo [*Chapman*, 1999] and Taussig [*Brian et al.*, 2005] Quadrangles, and indeed both coronae are sources for some of the youngest units. Only flows from a volcanic center located north-northeast of Atete clearly postdate this corona. Flows from Atete on its northern side are interbedded with those from Dhorani Corona (8° S, 243° E) [*Chapman*, 1999]. It is arguable from Figure 8 whether Dhorani is also active, although the evidence in favor is not compelling; in addition, it is possible that the oldest units of Atete are interbedded with the youngest flows from Dhorani. Maram Corona also appears to be young relative to other local units; only flows from Ledoux Patera postdate those from Maram [*Brian et al.*, 2005].

[23] This analysis indicates that 7 of the 215 coronae in this mapped region are active, and scaling this fraction to the total population would suggest that 17 coronae are active globally. We have previously estimated that each thermal possesses 10^{25}–10^{26} J of heat energy. If coronae do form over timescales of 1–10 Myr, then the power delivered to the surface of Venus from corona-forming thermals is currently ~0.5–50 TW. In comparison, the total rate of heat loss on Venus is ~20 TW (a global heat flux of ~45 mW m^{-2} [*Phillips and Hansen*, 1998] integrated over the surface). It is thus conceivable that a moderate fraction of the total heat loss on Venus is due to these thermals, which is broadly similar to the fraction of heat lost on the Earth from thermally buoyant plumes [e.g., *Davies and Richards*, 1992; *Sleep*, 1992].

[24] Gravity modeling is inherently nonunique, and it is certainly conceivable that other phenomena have produced the observed signals. Any positively buoyant feature in the mantle could give rise to the signals we predict; however, the magnitudes of the signals would be different because of the likely different density contrasts associated with other sources of buoyancy (e.g., compositional). It is the correspondence of signals of this length scale and these magnitudes with coronae otherwise inferred to be active that suggests we may have identified actively impinged thermals on the base of the lithosphere of Venus.

4. Discussion

[25] We contrast past models for corona formation with our scenario in light of the four critical observations presented in section 2. The first observation is the broad range of diameters. Analyses of relevant systems (e.g., mantle plumes and thermals arising from boundary layers [*Lithgow-Bertelloni et al.*, 2001] or formation of melt diapirs [*Tackley and Stevenson*, 1993]) demonstrate that the convective structures possess a size range much more restricted than the wide diameter range displayed for coronae (factor of ~2–3 versus factor of >16, or at least a factor of ~8 if the extreme members of the population are neglected). Unlike previous models [e.g., *Janes et al.*,

Table 2. Active Coronae in the BAT Region of Venus[a]

Name	Latitude, °N	Longitude, °E	Maximum Width, km	Average Width, km
—	19.5	265.5	150	150
—	−27.5	262.5	225	225
Aruru	9.0	262.0	450 × 350	400
Maram	−7.5	221.5	600 × 300	450
Atete	−16.0	243.5	600	600
Shiwanokia	−42.0	279.8	675	675
Zisa	12.0	221.0	850	850

[a]Corona information is from the database of *Stofan et al.* [2001] and *Glaze et al.* [2002]. BAT denotes the Beta, Atla, and Themis volcanic rises.

1992; *Koch and Manga*, 1996; *Smrekar and Stofan*, 1997; *Hansen*, 2003], our scenario is consistent with the wide range. While the thermals are of restricted sizes, the extent of melt that forms on top of the thermals as they impinge on the lithosphere should exhibit a much wider range, from essentially zero (i.e., no melt) to perhaps >1000 km (i.e., nearly the width of the impinged thermal), because the amount of melting is sensitive to local variables (Figure 4) [cf. *Farnetani et al.*, 1996, 2002]. The mean size (∼200–300 km) may thus reflect average conditions in the mantle and lithosphere of Venus.

[26] The second critical observation is the complex, varied topography, characterized by as many as nine distinct types [*Smrekar and Stofan*, 1997]. Most previous models explain only a subset of the topographic types [e.g., *Janes et al.*, 1992]. Indeed, only a few proposed models can yield those topographic types with central regions having elevations level with or below the background terrain [e.g., *Koch and Manga*, 1996; *Smrekar and Stofan*, 1997; *Hoogenboom and Houseman*, 2006]. *Smrekar and Stofan* [1997] suggest that their model can account for all the topographic types. These models, however, invoke an upwelling or downwelling originating from a boundary layer as being directly responsible for the corona, thereby likely failing to satisfy the first critical observation. In addition, these models neglect the presence of a mechanical lithosphere, its elastic equivalent likely tens of kilometers thick [e.g., *Johnson and Sandwell*, 1994; *Barnett et al.*, 2002; *Smrekar et al.*, 2003], and instead predict surface topography by isostatically balancing vertical flow stresses. Our conceptual model could plausibly give rise to the variety of topographic types, although this presumption remains to be thoroughly tested. The stochastic combination of magmatic underplating, intrusive and surface volcanism, subsurface density anomalies, lower crustal flow, and deformation of the mechanical lithosphere in response to these loads can nonetheless be expected to yield a complex and varied topographic signature. As demonstrated, a thermomechanical simulation of the proposed scenario, using simple plateau-shaped loads, yielded a topographic profile consistent with one of the more populous topographic classes of coronae.

[27] Many previous models also appear inconsistent with the third critical observation: the fracture annulus. To produce the pervasive fracturing, stresses of proper orientation and sufficient magnitude must be generated. In their fluid-flow analysis, *Koch and Manga* [1996] provided relationships for stress scaling at two times, during the initial impingement of a spherical plume head when stress orientations predict central radial fracturing, and a later phase when the plume head has flattened to ∼2–2.5 times its initial width and stress orientations predict a fracture annulus. During these times, maximum stresses are ∼10% and ∼1%, respectively, of a buoyancy stress scale factor $\Delta\rho ga$, where $\Delta\rho$ is the density contrast of the plume head with the mantle, g is gravitational acceleration (8.87 m s^{-2}), and a is the radius of the plume head. For direct formation of a corona via impingement of a thermally buoyant plume head, we consider an extreme case and a case more typical for the corona population. The largest corona, Artemis, is ∼2600 km in diameter, which is over twice as wide as the next largest corona, and given its size and complex geology, its genetic linkage to the rest of the population is not assured [e.g., *Glaze et al.*, 2002; *Hansen*, 2003]. In fluid impingement models, a corona 2600 km in diameter would require a plume head ∼1000–1300 km across, or a = 500–650 km. Thermally buoyant plumes are likely several hundred Kelvin hotter than the ambient mantle [e.g., *Farnetani et al.*, 2002]; for an extreme upper bound of 500 K (to maximize stresses), $\Delta\rho$ is at most ∼50 kg m^{-3} for a volumetric thermal expansion coefficient of 3 × 10^{-5} K^{-1}. Maximum stresses during the two phases are thus ∼30 MPa and ∼3 MPa. Examination of tectonic features on Venus, however, indicates fault strengths of 10 to perhaps 80 MPa [*Barnett and Nimmo*, 2002], so formation of the characteristic fracture annulus is doubtful, even in this extreme case. For a more typical case with a = 125 km and an excess temperature of 300 K, maximum stresses during the two phases are then ∼3 MPa and ∼0.3 MPa. For thermal buoyancy, therefore, the fluid-flow-based model of *Koch and Manga* [1996] fails to predict sufficient stress magnitudes. Though not discussed, stresses in the work of *Smrekar and Stofan* [1997] and *Hoogenboom and Houseman* [2006] are likely similar, as all three models are based on fluid-flow analyses and isostatically translate vertical flow stresses into topography of comparable heights. Compositional buoyancy (melt) could generate stresses an order of magnitude greater than for thermal plumes, but such levels are still not sufficient to produce concentric fracturing for mean-size coronae. On the other hand, models that incorporate deformation of an elastic lithosphere, particularly peripheral flexing in response to a surface load [e.g., *Janes et al.*, 1992; *Johnson and Sandwell*, 1994], predict appropriately oriented stresses of several hundred MPa. In addition, flexure of a mechanical lithosphere locally thinned by magmatism may result in a distinct annulus

of large stresses (Figure 7c) [cf. *Dombard and Phillips*, 2005]. Thus deformation of the mechanical lithosphere in response to the proposed loads could lead to the formation of fracture annuli.

[28] The last critical observation is the significant role of volcanism. While volcanism is not a primary component of many models [see *Stofan et al.*, 1997, Figure 8], it is perhaps the most crucial element of our hypothesis. Extensive surface flows are evident for a substantial portion of the corona population (at least 41%), perhaps a majority if potential observational biases are considered [*Roberts and Head*, 1993], and coronal flows are a major contributor to the resurfacing of Venus [*Stofan et al.*, 2005]. Furthermore, limited surface flows do not preclude extensive magmatic intrusion, because of the large ratio of intrusive to extrusive magmatic volumes for analogous systems on Earth [e.g., *Crisp*, 1984]. Indeed, this element of our conceptual model is driven by terrestrial analogy. When evident, surface flows from some coronae cover areas of 10^4–10^6 km^2, comparable to the spatial extent of terrestrial flood basalts [*Stofan et al.*, 2005]. Radially oriented fracture centers on Venus, interpreted as radiating dike swarms [*Ernst et al.*, 1995; *Grindrod et al.*, 2005], are associated with both volcanic rises and coronae; on Earth, giant radiating dike swarms are associated with large igneous provinces, which are inferred to mark the impingement of a thermally buoyant mantle plume head on the lithosphere [e.g., *Richards et al.*, 1989; *Ernst et al.*, 1995]. That radiating dike swarms are associated with both volcanic rises and coronae on Venus suggests that these features also form from plume-induced volcanism.

5. Concluding Remarks

[29] We have presented a conceptual model for the formation of a corona on Venus as the response to magmatic loading of the crust by the upward transport of melt from the top of a transient mantle plume or thermal. In contrast to past models, this model ties together four critical observations of coronae on Venus. Because the model is schematic, however, uncertainties remain and further analysis is warranted. For instance, the model may be consistent with the observation of a concentration of coronae near chasmata. It is possible that chasmata form from tractions on the lithosphere arising from large-scale mantle flow that also focuses the ascent of thermals, indicating that coronae and chasmata are associated but not causally related, such as has been observed near Parga Chasma [*Martin et al.*, 2005]. In addition, a future, more thorough, global investigation of the topography and gravity, coupled with additional geologic mapping, may reveal additional active coronae. Petrological questions regarding melt buoyancy within the upper mantle of Venus are difficult to constrain, but terrestrial analogies confirm plausibility [*Farnetani et al.*, 1996; *Spiegelman et al.*, 2001]. A critical question is how to explain morphologic differences between coronae and volcanoes on Venus; this difference could be due to the large effusion rates and possible compositional variations associated with larger degrees of partial melt over an impinging thermal upwelling, in analogy to the difference between large igneous provinces (i.e., from plume heads) and hot-spot volcanoes (i.e., from plume tails) on Earth [e.g., *Richards et al.*, 1989]. To continue the analogy, the distinction between large igneous provinces and coronae could be the result of a stagnant lithosphere, thick basaltic crust, and high temperatures at the base of the crust on Venus. Furthermore, it may be difficult to reconcile this model with observations of coronae with limited surface volcanism, tectonic signatures dominated by subsurface inflation instead of top-loaded flexure, or both, as is often found for coronae near Parga Chasma [*Martin et al.*, 2005]; one possibility is a larger-than-average ratio of intrusive to extrusive volcanism. Clearly, improved understanding could be provided by fully integrated numerical models that add melt migration and intrusion processes to basic thermal convection and primary partial melting, a difficult task involving multiple sets of governing equations and requiring resolution over both large (>100 km) and small (<1 km) length scales. Moreover, additional detailed thermomechanical modeling is needed to test more thoroughly that the time-dependent effects of melt buoyancy, crustal underplating and intrusion, surface volcanism, crustal thinning, and deformation of the mechanical lithosphere reproduces the full range of topographic and tectonic characteristics observed within the corona population.

[30] **Acknowledgments.** We thank Francis Nimmo for discussions on lower crustal flow, Steven Hauck and Mark Jellinek for discussions about melting, Rebecca Ghent for instructive advice on the geology of Venus, and Norman Sleep and Ellen Stofan for critical reviews that helped us to refine our arguments. This research has been supported by the NASA Planetary Geology and Geophysics Program under grants NAG5-10165 and NNG04G164G (to S.C.S.), NAG5-11563 and NNG05GK34G (to C.L.J.), and NNG05GQ81G (to Roger J. Phillips). The preparation of this paper was supported in part by the Johns Hopkins University Applied Physics Laboratory (A.J.D.) and the Institut de Physique du Globe de Paris (C.L.J.).

References

Banerdt, W. B. (1986), Support of long-wavelength loads on Venus and implications for internal structure, *J. Geophys. Res.*, *91*, 403–419.

Barnett, D. N., and F. Nimmo (2002), Strength of faults on Mars from MOLA topography, *Icarus*, *157*, 34–42.

Barnett, D. N., F. Nimmo, and D. McKenzie (2002), Flexure of Venusian lithosphere measured from residual topography and gravity, *J. Geophys. Res.*, *107*(E2), 5007, doi:10.1029/2000JE001398.

Beck, A. R., Z. T. Morgan, Y. Liang, and P. C. Hess (2006), Dunite channels as viable pathways for mare basalt transport in the deep lunar mantle, *Geophys. Res. Lett.*, *33*, L01202, doi:10.1029/2005GL024008.

Brian, A. W., E. R. Stofan, and J. E. Guest (2005), Geologic map of the Taussig Quadrangle (V-39), Venus, *Map 2813*, U. S. Geol. Surv., Denver, Colo.

Caress, D. W., M. K. McNutt, R. S. Detrick, and J. C. Mutter (1995), Seismic imaging of hotspot-related crustal underplating beneath the Marquesas Islands, *Nature*, *373*, 600–603.

Chapman, M. G. (1999), Geologic/geomorphic map of the Galindo Quadrangle (V-40), Venus, *Map 2613*, U. S. Geol. Surv., Denver, Colo.

Crisp, J. A. (1984), Rates of magma emplacement and volcanic output, *J. Volcanol. Geotherm. Res.*, *20*, 177–211.

Cyr, K. E., and H. J. Melosh (1993), Tectonic patterns and regional stresses near Venusian coronae, *Icarus*, *102*, 175–184.

Davaille, A., and J. Vatteville (2005), On the transient nature of mantle plumes, *Geophys. Res. Lett.*, *32*, L14309, doi:10.1029/2005GL023029.

Davies, G. F., and M. A. Richards (1992), Mantle convection, *J. Geol*, *100*, 151–206.

Diakov, S., R. West, D. Schissel, A. Krivtsov, V. Kochnev-Peroukhov, and I. Migachev (2002), Recent advances in the Noril'sk model and its application for exploration of Ni-Cu-PGE sulfide deposits, *Soc. Econ. Geol. Spec. Publ.*, *9*, 203–226.

Dombard, A. J., and W. B. McKinnon (2006a), Elastoviscoplastic relaxation of impact crater topography with application to Ganymede and Callisto, *J. Geophys. Res.*, *111*, E01001, doi:10.1029/2005JE002445.

Dombard, A. J., and W. B. McKinnon (2006b), Folding of Europa's icy lithosphere: An analysis of viscous-plastic buckling and subsequent topographic relaxation, *J. Struct. Geol.*, *28*, 2259–2269.

Dombard, A. J., and R. J. Phillips (2005), Tectonic evidence for crustal underplating of the Tharsis Montes, Mars [CD-ROM], *Lunar Planet. Sci., XXXVI*, abstract 1878.

Dombard, A. J., C. L. Johnson, M. A. Richards, and S. C. Solomon (2002), A transient plume melting model for coronae on Venus [CD-ROM], *Lunar Planet. Sci., XXXIII*, abstract 1877.

Dombard, A. J., C. L. Johnson, M. A. Richards, and S. C. Solomon (2006), Coronae on Venus as products of magmatic loading of the crust over transient plume heads: Consequences for surface deformation and volcanism, paper presented at Chapman Conference on Exploring Venus as a Terrestrial Planet, AGU, Key Largo, Fla.

Ernst, R. E., J. W. Head, E. Parfitt, E. Grosfils, and L. Wilson (1995), Giant radiating dyke swarms on Earth and Venus, *Earth Sci. Rev.*, *39*, 1–58.

Farnetani, C. G., M. A. Richards, and M. S. Ghiorso (1996), Petrological models of magma evolution and deep crustal structure beneath hotspots and flood basalt provinces, *Earth Planet. Sci. Lett.*, *143*, 81–94.

Farnetani, C. G., B. Legras, and P. J. Tackley (2002), Mixing and deformations in mantle plumes, *Earth Planet. Sci. Lett.*, *196*, 1–15.

Glaze, L. S., E. R. Stofan, S. E. Smrekar, and S. M. Baloga (2002), Insights into corona formation through statistical analyses, *J. Geophys. Res.*, *107*(E12), 5135, doi:10.1029/2002JE001904.

Gonnermann, H. M., A. M. Jellinek, M. A. Richards, and M. Manga (2004), Modulation of mantle plumes and heat flow at the core mantle boundary by plate-scale flow: Results from laboratory experiments, *Earth Planet. Sci. Lett.*, *226*, 53–67.

Grimm, R. E., and P. C. Hess (1997), The crust of Venus, in *Venus II*, edited by S. W. Bougher, D. M. Hunten, and R. J. Phillips, pp. 1205–1244, Univ. of Ariz. Press, Tucson.

Grindrod, P. M., F. Nimmo, E. R. Stofan, and J. E. Guest (2005), Strain at radially fractured centers on Venus, *J. Geophys. Res.*, *110*, E12002, doi:10.1029/2005JE002416.

Hansen, V. L. (2003), Venus diapirs: Thermal or compositional?, *Geol. Soc. Am. Bull.*, *115*, 1040–1052.

Hirschmann, M. M. (2000), Mantle solidus: Experimental constraints and the effects of peridotite composition, *Geochem. Geophys. Geosyst.*, *1*(10), doi:10.1029/2000GC000070.

Hoogenboom, T., and G. A. Houseman (2006), Rayleigh-Taylor instability as a mechanism for corona formation on Venus, *Icarus*, *180*, 292–307.

Hoogenboom, T., S. E. Smrekar, F. S. Anderson, and G. Houseman (2004), Admittance survey of type 1 coronae on Venus, *J. Geophys. Res.*, *109*, E03002, doi:10.1029/2003JE002171.

Janes, D. M., S. W. Squyres, D. L. Bindschadler, G. Baer, G. Schubert, V. L. Sharpton, and E. R. Stofan (1992), Geophysical models for the formation and evolution of coronae on Venus, *J. Geophys. Res.*, *97*, 16,055–16,067.

Jellinek, A. M., and M. Manga (2004), Links between long-lived hot spots, mantle plumes, D'', and plate tectonics,, *Rev. Geophys.*, *42*, RG3002, doi:10.1029/2003RG000144.

Jellinek, A. M., A. Lenardic, and M. Manga (2002), The influence of interior mantle temperature on the structure of plumes: Heads for Venus, tails for the Earth, *Geophys. Res. Lett.*, *29*(11), 1532, doi:10.1029/2001GL014624.

Jellinek, A. M., H. M. Gonnermann, and M. A. Richards (2003), Plume capture by divergent plate motions: Implications for the distribution of hotspots, geochemistry of mid-ocean ridge basalts, and estimates of the heat flux at the core-mantle boundary, *Earth Planet. Sci. Lett.*, *205*, 361–378.

Johnson, C. L., and M. A. Richards (2003), A conceptual model for the relationship between coronae and large-scale mantle dynamics on Venus, *J. Geophys. Res.*, *108*(E6), 5058, doi:10.1029/2002JE001962.

Johnson, C. L., and D. T. Sandwell (1994), Lithospheric flexure on Venus, *Geophys. J. Int.*, *119*, 627–647.

Karato, S.-I., and P. Wu (1993), Rheology of the upper mantle: A synthesis, *Science*, *260*, 771–778.

Koch, D. M., and M. Manga (1996), Neutrally buoyant diapirs: A model for Venus coronae, *Geophys. Res. Lett.*, *23*, 225–228.

Lawrence, K. P., and R. J. Phillips (2003), Gravity/topography admittance inversion on Venus using niching genetic algorithms, *Geophys. Res. Lett.*, *30*(19), 1994, doi:10.1029/2003GL017515.

Leitch, A. M., and G. F. Davies (2001), Mantle plumes and flood basalts: Enhanced melting from plume ascent and an eclogite component, *J. Geophys. Res.*, *106*, 2047–2059.

Lithgow-Bertelloni, C., M. A. Richards, C. P. Conrad, and R. W. Griffiths (2001), Plume generation in natural thermal convection at high Rayleigh and Prandtl numbers, *J. Fluid Mech.*, *434*, 1–21.

Mackwell, S. J., M. E. Zimmerman, and D. L. Kohlstedt (1998), High-temperature deformation of dry diabase with application to tectonics on Venus, *J. Geophys. Res.*, *103*, 975–984.

Martin, P., E. R. Stofan, and L. S. Glaze (2005), Analysis of coronae in the Parga Chasma region, Venus [CD-ROM], *Lunar Planet. Sci.*, *XXXVI*, abstract 1617.

Nimmo, F., and D. J. Stevenson (2001), Estimates of Martian crustal thickness from viscous relaxation of topography, *J. Geophys. Res.*, *106*, 5085–5098.

Nunes, D. C., R. J. Phillips, C. D. Brown, and A. J. Dombard (2004), Relaxation of compensated topography and the evolution of crustal plateaus on Venus, *J. Geophys. Res.*, *109*, E01006, doi:10.1029/2003JE002119.

Phillips, R. J., and V. L. Hansen (1998), Geological evolution of Venus: Rises, plains, plumes, and plateaus, *Science*, *279*, 1492–1497.

Pritula, Y. A., K. A. Savinsky, A. B. Kogan, T. G. Smirnova, and I. M. Shtutin (1974), Structure of terrestrial crust in Tunguska syncline, *Int. Geol. Rev.*, *16*, 1144–1152.

Richards, M. A., R. A. Duncan, and V. E. Courtillot (1989), Flood basalts and hotspot tracks: Plume heads and tails, *Science*, *246*, 103–107.

Roberts, K. M., and J. W. Head (1993), Large-scale volcanism associated with coronae on Venus: Implications for formation and evolution, *Geophys. Res. Lett.*, *20*, 1111–1114.

Robin, C. M., V. Thalayan, and A. M. Jellinek (2004), Experimental study of transient thermal convection following a catastrophic lithospheric overturn: Applications to the tectonic style, thermal evolution and topography of Venus,, *Eos Trans. AGU*, *85*, Spring Meet. Suppl., abstract P33D-11.

Robin, C. M., V. Thalayan, and A. M. Jellinek (2006), Implications of transient convection for Venusian geodynamics, paper presented at Chapman Conference on Exploring Venus as a Terrestrial Planet, AGU, Key Largo, Fla..

Simons, M., S. C. Solomon, and B. H. Hager (1997), Localization of gravity and topography: Constraints on the tectonics and mantle dynamics of Venus, *Geophys. J. Int.*, *131*, 24–44.

Sleep, N. H. (1992), Hotspot volcanism and mantle plumes, *Annu. Rev. Earth Planet. Sci.*, *20*, 19–43.

Sleep, N. H., C. J. Ebinger, and J.-M. Kendall, (2002), Deflection of mantle plume material by cratonic keels, in *The Early Earth: Physical, Chemical and Biological Development*, edited by C. M.R. Fowler, C. J. Ebinger, and C. J. Hawkesworth, *Geol. Soc. Spec. Publ.*, *199*, 135–150.

Smrekar, S. E., and E. R. Stofan (1997), Corona formation and heat loss on Venus by coupled upwelling and delamination, *Science*, *277*, 1289–1294.

Smrekar, S. E., and E. R. Stofan (1999), Origin of corona-dominated topographic rises on Venus, *Icarus*, *139*, 100–115.

Smrekar, S. E., W. S. Kiefer, and E. R. Stofan (1997), Large volcanic rises on Venus, in *Venus II*, edited by S. W. Bougher, D. M. Hunten, and R. J. Phillips, pp. 845–878, Univ. of Ariz. Press, Tucson.

Smrekar, S. E., R. Comstock, and F. S. Anderson (2003), A gravity survey of Type 2 coronae on Venus, *J. Geophys. Res.*, *108*(E8), 5090, doi:10.1029/2002JE001935.

Solomatov, V. S., and L.-N. Moresi (1996), Stagnant lid convection on Venus, *J. Geophys. Res.*, *101*, 4737–4754.

Spiegelman, M., P. B. Kelemen, and E. Aharonov (2001), Causes and consequences of flow organization during melt transport: The reaction infiltration instability in compactible media, *J. Geophys. Res.*, *106*, 2061–2077.

Stofan, E. R., and S. E. Smrekar (2005), Large topographic rises, coronae, large flow fields, and large volcanoes on Venus: Evidence for mantle plumes?, in *Plates, Plumes, and Paradigms*, edited by G. R. Foulger et al., *Spec. Pap. Geol. Soc. Am.*, 388, 841–861.

Stofan, E. R., V. L. Sharpton, G. Schubert, G. Baer, D. L. Bindschadler, D. M. Janes, and S. W. Squyres (1992), Global distribution and characteristics of coronae and related features on Venus: Implications for origin and relation to mantle processes, *J. Geophys. Res.*, *97*, 13,347–13,378.

Stofan, E. R., S. E. Smrekar, D. L. Bindschadler, and D. A. Senske (1995), Large topographic rises on Venus: Implications for mantle upwelling, *J. Geophys. Res.*, *100*, 23,317–23,327.

Stofan, E. R., V. E. Hamilton, D. M. Janes, and S. E. Smrekar (1997), Coronae on Venus: Morphology and origin, in *Venus II*, edited by S. W. Bougher, D. M. Hunten, and R. J. Phillips, pp. 931–965, Univ. of Ariz. Press, Tucson.

Stofan, E. R., S. E. Smrekar, S. W. Tapper, J. E. Guest, and P. M. Grindrod (2001), Preliminary analysis of an expanded corona database for Venus, *Geophys. Res. Lett.*, *28*, 4267–4270.

Stofan, E. R., A. W. Brian, and J. E. Guest (2005), Resurfacing styles and rates on Venus: Assessment of 18 Venusian quadrangles, *Icarus*, *173*, 312–321.

Tackley, P. J., and D. J. Stevenson (1991), The production of small Venusian coronae by Rayleigh-Taylor instabilities in the uppermost mantle, *Eos Trans. AGU*, *72*(44), Fall Meet. Suppl., 287.

Tackley, P. J., and D. J. Stevenson (1993), A mechanism for spontaneous self-perpetuating volcanism on the terrestrial planets, in *Flow and Creep in the Solar System: Observations, Modeling, and Theory*, edited by D. B. Stone and S. K. Runcorn, pp. 307–321, Springer, New York.

Turcotte, D. L., and G. Schubert (1982), *Geodynamics*, John Wiley, Hoboken, N. J.

Watson, S., and D. McKenzie (1991), Melt generation by plumes: A study of Hawaiian volcanism, *J. Petrol.*, *32*, 501–537.

Wieczorek, M. A., and R. J. Phillips (1998), Potential anomalies on a sphere: Applications to the thickness of the lunar crust, *J. Geophys. Res.*, *103*, 1715–1724.

A. J. Dombard (corresponding author), Planetary Exploration Group, Space Department, Johns Hopkins University Applied Physics Laboratory, 11100 Johns Hopkins Rd., Laurel, MD 20723, USA. (andrew.dombard@jhuapl.edu)

C. L. Johnson, Department of Earth and Ocean Sciences, University of British Columbia, 6339 Stores Road, Vancouver, BC, Canada V6T 1Z4.

M. A. Richards, Department of Earth and Planetary Science, University of California, Berkeley, CA 94270, USA.

S. C. Solomon, Department of Terrestrial Magnetism, Carnegie Institution of Washington, Washington, D.C., 20015, USA.